JOURNAL OF CATALYSIS 139, 62–71 (1993)

Unsteady-State Carbon Monoxide Methanation on an Ni/SiO_2 Catalyst

VLADIMÍR STUCHLÝ AND KAREL KLUSÁČEK*

Institute of Chemical Process Fundamentals, Czechoslovak Academy of Sciences, Rozvojova 135, 165 02 Prague 6, Czechoslovakia

Received December 4, 1990; revised June 1, 1992

Carbon monoxide methanation on a commercial Ni/SiO_2 catalyst has been investigated by transient kinetic methods. It was found that carbon monoxide blocks the adsorption of hydrogen and replaces it on the catalyst surface. Oxygenated and non-oxygenated reaction intermediates were found on the catalyst surface between 458 and 538 K, in amounts exceeding severalfold the monolayer coverage. This extensive deposition was due to the presence of hydrogen in the gaseous phase. The volume deposits was unreactive under steady-state reaction conditions but reactive under dynamic conditions. Therefore, the reaction scheme proposed to describe the observed system behavior includes steady-state and unsteady-state reaction steps. Two types of activity sites, a substitution mechanism of CO adsorption, the storage of intermediates on sites other than reaction ones, and their variable concentration depending on the reaction conditions are considered. 1993 Academic Press, Inc.

INTRODUCTION

There is a controversy in the literature between the steady-state reaction schemes of catalytic carbon monoxide methanation and the results of unsteady-state kinetic measurements. Recent unsteady-state concentration-programmed reaction (CPR) and temperature-programmed reaction (TPR) measurements have revealed phenomena that are not included in the steady-state methanation kinetic schemes and models.

Following the step exchange of hydrogen for the CO/H_2 methanation reaction mixture (CPR start-up experiments), a monotonic increase of the methanation rate to a steady-state value was observed by Mori *et al.* (*1*), Underwood and Bennett (*2*), and Lee and Schwartz (*3*) on nickel catalysts. However, a small overshoot in methane (water) concentration was reported on nickel (*4*) and ruthenium-based (*5*) catalysts, and an initial increase in catalytic activity with slow subsequent decline was found on clean iron at higher reaction temperatures (*6*). Biloen and Sachtler (*7*) suggested that the reactive carbidic carbon (CH_x, $x = 0$–3) was probably built up during the rise of activity and the unreactive, graphitic carbon was formed concurrently with the catalyst activity decline.

The simultaneous monitoring of both reaction products, methane and water, has brought information about the relative rates of the C–O bond splitting step and the hydrogenation steps. Following the switch from hydrogen to CO/H_2 methanation mixture on nickel catalysts, methane and water were always produced at the same rate (*1*, *5*). This result indicated that the C–O bond dissociation, probably of the adsorbed CO, was the rate-controlling step of the methane formation (*1*). On the other hand, the formation of CO_2 (by the reaction of adsorbed CO with surface oxygen from CO dissociation) preceded the formation of CH_4, indicating that CO disproportionation was fast compared to hydrogenation of active carbon from CO dissociation (*8*). Goodman *et al.* (*9*) found that rates of CO disproportionation and carbon hydrogenation were comparable with the rate of methanation. They

* To whom correspondence should be addressed.

0021-9517/93 $5.00

concluded that there was no unambiguous rate-determining step in the methanation reaction (*9*).

In contrast to start-up experiments, the abrupt removal of CO from CO/H_2 methanation feed (CPR stop experiments) at moderate temperatures is always characterized by a sharp (and transient) increase in CH_4 production, followed by a gradual decline to zero (*2, 5, 7, 10, 11, 14*). An explanation of these phenomena has been derived from the fact that H_2 competes poorly with CO for adsorption sites on the catalyst surface. Removal of CO from the gaseous phase uncovers the surface for hydrogen adsorption, and hydrogenation of carbonaceous precursors of methane becomes possible (*7, 10*). The amount of CH_4 formed during the transient may exceed the amount corresponding to monolayer coverage by more than an order of magnitude, indicating that under steady-state (or during the start-up period) a reservoir of carbonaceous species is built up equivalent to several layers of carbon (*13, 14*). Both the carbidic reaction products and the carbonaceous side products (not reaction intermediates) are assumed to be converted to methane after the switch of reactor feed to pure hydrogen (*10*).

Evolution of the other reaction product, water, has also been followed during the exchange of CO/H_2 mixture for hydrogen (*2, 4, 5*), in order to find out the surface concentration of non-oxygenated methane precursors. The amount of methane evolved always significantly exceeded the amount of water, indicating the presence of a substantial amount of nonoxygenated species, probably carbidic in nature. The carbidic carbon is hydrogenated faster than CO (see Refs. (*2, 4, 5, 14*)) and it is therefore supposed to be the principal steady-state reaction intermediate.

A step change of feed composition from CO/inert gaseous mixture to hydrogen or water (*15, 16*) (and vice versa) has been studied in an effort to reveal the possible reaction pathway of CO during methanation. Upon switching to H_2, the methane response was similar to that obtained after reaction with CO/H_2, indicating that under methanation conditions, CO reacts similarly (*2, 5*). Methane was again formed due to hydrogenation of surface non-oxygenated carbidic material as well as surface oxygenated carbonaceous species (*2, 5*). The deposition of carbon was much easier in the presence of hydrogen. This was explained in terms of indirect hydrogen assistance to the C–O bond breaking, by removal of surface oxygen (*2, 5*). However, a direct participation of hydrogen in this step is also assumed (*4, 10*).

In another group of experiments, transient and steady-state isotopic tracing with ^{13}C, ^{18}O, and D has been utilized to understand the reaction mechanism of CO methanation. Dalla Betta and Shelef (*17*) found no deuterium isotope effect on Ni, Ru, and Pt catalysts. An inverse isotope effect of deuterium has been found more often (*1, 18, 19*) and has been interpreted as indication of the absence of hydrogen in the C–O breaking step (*1*) and as a support for the slow addition of hydrogen to surface hydrogenated CH_x species (*18, 19*). On the basis of their experiments with ^{13}CO, Araki and Ponec (*8*) have postulated that methanation proceeds via active carbon hydrogenation in the slow step. This conclusion has been later supported and extended by Biloen *et al.* (*20, 21*), Happel *et al.* (*22, 23*), Galuszka *et al.* (*24*), Cant and Bell (*5*), and Coenen *et al.* (*11*). They have found that not only C, but also surface CH intermediates could be hydrogenated in the rate-controlling steps of methanation.

TPR methods have also been employed to study the reactivity and the surface population of possible reaction intermediates. When a nickel catalyst was saturated by CO and H_2 at ambient temperature, then during the temperature increase in inert atmosphere, methane left the catalyst simultaneously with water (*25*). The same temperature of methane and water evolution indicated that C–O bond breaking determined the rate of methanation. After expo-

sure of nickel catalyst to CO/H_2 and CO/He mixtures at higher temperatures (*26*), methane was evolved in two peaks but water accompanied only the second methane peak. This implied (26) that active carbon as well as adsorbed CO were present on the catalyst surface and that reactivity of the active carbon was higher than that of CO.

TPR studies of hydrogenation of surface carbonaceous deposits by gas-phase hydrogen (*26–31*) have confirmed the higher methanation activity of non-oxygenated carbidic deposits in comparison with adsorbed CO. The results indicate that at high surface coverages, carbon hydrogenation is not rate-determining for CO hydrogenation in excess of hydrogen (*26*). The existence of various forms of surface reactive carbon has also been proved by TPR measurements (e.g., Refs. (*28–31*)). Although some of them exhibit low reactivity to produce methane under common methanation conditions, two different types of carbon which can react were assumed (*30*).

This brief review of transient kinetic studies on CO methanation illustrates that steady-state methanation reaction schemes and kinetic models, although sufficient to describe the steady-state reaction behavior, may not be valid under unsteady-state reaction conditions, owing to the complexity of the methanation reaction. It is the aim of this contribution to investigate the adsorption/desorption behavior of reaction components and the formation, surface concentrations, and reactivity of the methanation reaction intermediates. On this basis, a reaction scheme is proposed which considers the observed unsteady-state reaction behavior.

EXPERIMENTAL

A commercial, 29 wt% Ni/SiO_2 catalyst G-33 (Girdler Südchemie, FRG; for properties, see Table 1) was crushed into 0.16–0.25 mm particles and activated for 2 hr at 623 K in a flow of hydrogen. Experiments were performed in a tubular flow microreactor (volume about 1 cm^3) equipped with a thin thermocouple inserted into the catalyst bed (50–100 mg) to measure its temperature precisely. The reaction components, CO, H_2, and argon, were introduced into the reactor after purification and by means of the mass flow controllers. The furnace temperature was controlled independently by a PID programmable controller. The reactor effluent was analyzed by a Balzers QMS 420 on-line quadrupole mass spectrometer.

TABLE 1

Properties of the G-33 Catalyst

Ni content (wt%)	29
Surface area[a] ($m^2\ g^{-1}$)	112
Particle diameter (mm)	0.16–0.25
Pore volume[a] ($cm^3\ g^{-1}$)	0.134
Bulk density[b] ($g\ cm^{-3}$)	1.73
Apparent density[b] ($g\ cm^{-3}$)	2.84
Helium density ($g\ cm^{-3}$)	3.10
Porosity	0.52
Most frequent pore radius[a] (nm)	40

[a] BET.
[b] Mercury porosimetry.

Dynamic adsorption measurements were performed at ambient temperature, by admitting pulses (volume 0.086 cm^3) of hydrogen or CO in argon to activated catalyst. Prior to measurement, the catalyst was treated in argon at 623 K for 30 min to remove hydrogen and water from the preceding activation procedure.

TPD (temperature-programmed desorption) and TPSR (temperature programmed surface reaction) experiments were carried out following saturation of the activated catalyst surface by H_2, 3% of CO in H_2, or 3% of CO in Ar mixture at ambient temperature. The catalyst was then flushed for 10 min with Ar (42 cm^3/min) and its temperature was gradually increased in flowing argon at the rate of 15 K min^{-1}.

CPR (concentration-programmed reaction) experiments were performed either by switching between CO/Ar and H_2 streams or between CO/H_2 and H_2 streams, in the temperature range 458–538 K. The step change of the feed composition was achieved by switching two carefully bal-

TABLE 2

Adsorption Capacity of the G-33 Catalyst for CO and H_2 at 300 K

Adsorption procedure	Adsorption capacity (μmol g^{-1})	
	CO	H_2
H_2 adsorption	—	109
CO adsorption	110	—
CO adsorbed after H_2	120	68[a]
H_2 adsorbed after CO	110[b]	42

[a] Remainder after adsorption of CO.
[b] Remainder after adsorption of H_2.

anced streams with different reactant composition, using a system of programmable six-way valves. The switching caused temperature changes of the catalyst due to the highly negative adsorption and reaction enthalpies. Using either low CO concentrations or low reaction temperatures, this effect has usually been less than ±5 K.

The composition of the reaction mixture leaving the reactor was followed by means of a calibrated Balzers QMS 420 quadrupole mass, spectrometer. Masses 2, 15, 18, 28, 40, and 44 were scanned corresponding to H_2, CH_3 (methyl), H_2O, CO, Ar (inert), and CO_2, respectively, at rates of 1–50 scans/sec. Only traces of CO_2 were detected at higher reaction temperatures. The time coordinate was corrected for transport lags (3–5 sec). The rate of concentration step change between Ar and H_2 (volumetric flowrate 100 cm^3 min^{-1}) was characterized by τ_{95} = 1 sec, where τ_{95} is the time within which the argon concentration reached 95% of its final value.

RESULTS AND DISCUSSION

Dynamic Adsorption Measurements

The results of pulse dynamic adsorption measurements at ambient temperature are summarized in Table 2. The catalyst adsorption capacity was measured for CO and H_2 on a clean catalyst surface (activated and then flushed with Ar at 623 K), and by preadsorption of CO followed by adsorption of H_2, and vice versa. The hydrogen uptake (109 μmol g^{-1}) corresponds to the number of surface Ni atoms (*32*) and was thus taken as the monolayer coverage. The catalyst had similar capacities for adsorption of CO (Table 2). When H_2 was preadsorbed, the amount of CO adsorbed remained practically unchanged. The adsorption of CO caused desorption of H_2 (Table 2) due to displacement of H_2 by CO. The opposite effect, i.e., CO desorption due to H_2 adsorption, was not observed, as CO is adsorbed more strongly than hydrogen (*12*). When hydrogen was adsorbed following the CO adsorption, hydrogen adsorption capacity was reduced below half of that for the clean catalyst surface. CO thus strongly blocked hydrogen adsorption and was capable of displacing hydrogen on a part of the catalyst surface. This may indicate that there is more than one type of hydrogen and carbon monoxide adsorption sites.

Temperature-Programmed Experiments

In order to investigate the adsorption of CO and H_2 further, temperature-programmed desorption (TPD) and surface reaction (TPSR) of CO and H_2 were performed. The results are given in Figs. 1–3. Figure 1 shows carbon monoxide desorption spectra from catalyst samples on which CO was adsorbed at ambient temperature from CO/Ar mixture (TPD, curve 1), when CO was coadsorbed with H_2 (TPSR, curve 2), when hydrogen was adsorbed consequently to the CO adsorption (TPSR, curve 3), and when the adsorption of hydrogen preceded the adsorption of CO (TPSR, curve 4). The desorption of CO during TPD was characterized by a TPD spectrum with two overlapping peaks (see e.g., Ref. (*25*)) with maxima at about 337 and 420 K, respectively. Their existence provides evidence for the presence of at least two adsorbed forms of CO. The CO desorption pattern was similar for all hydrogen-treated catalyst samples during TPSR (curves 2–4), but was strik-

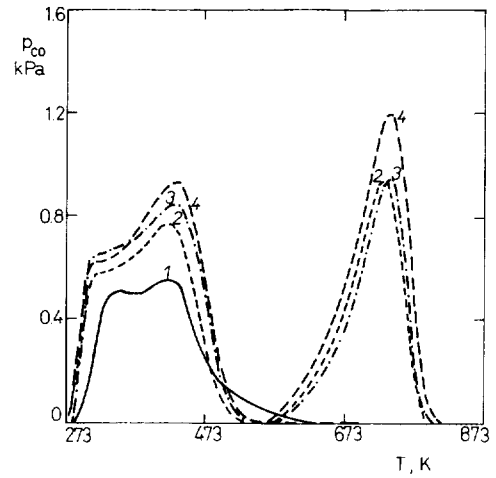

FIG. 1. Influence of the adsorption mode on desorption of CO. CO was adsorbed as follows: (1) × 2, from 3% CO/Ar mixture; (2) from 3% CO/H_2 mixture; (3) by admitting 3% CO/Ar followed by H_2 adsorption; (4) by H_2 adsorption followed by adsorption of CO from 3% CO/Ar.

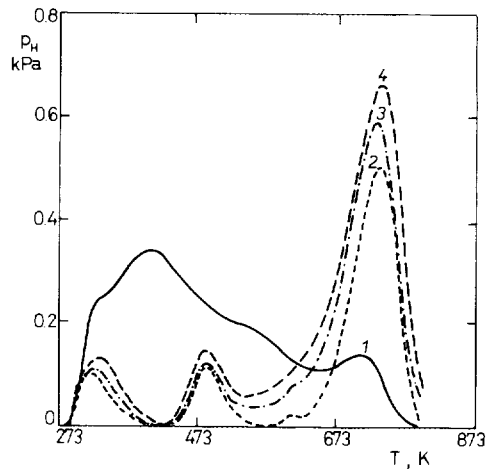

FIG. 2. Influence of the adsorption mode on desorption of H_2. H_2 was adsorbed as follows: Curve (1) × 0.5, by admitting H_2; (2) from 3% CO/H_2 mixture; (3) by admitting 3% CO/Ar followed by saturation by H_2 (4) by H_2 saturation followed by adsorption of CO from 3% CO/Ar.

ingly different from the TPD pattern (curve 1). In the low-temperature part of the TPSR spectra, the first peak was at lower temperature (310 K) than in the TPD, and in the region of high temperatures, a new large peak of CO (about 720 K) was detected. This indicates that adsorption of H_2 has a significant qualitative effect on the CO adsorption, mainly in the range of strong CO adsorption. By comparison of the data in Tables 2 and 3, it is evident that less than one-quarter of the adsorbed CO is subsequently desorbed when no hydrogen is present. The coadsorption of H_2 increases this amount more than four times (Table 3). Therefore, hydrogen facilitates the CO desorption at low temperatures and initiates a new strong CO interaction with the catalyst.

TABLE 3

Amounts of Reaction Components Evolved during TPD and TPSR

Procedure	Amount evolved (μmol g^{-1})			
	CO	H_2	CH_4	H_2O
TPD of CO	25	—	—	—
TPD of H_2	—	102	—	—
TPSR	104	35	3.2	3.0

This interaction is likely to be due to formation of a surface intermediate containing hydrogen, as seen from the simultaneous occurrence of high-temperature peaks in Figs. 1 and 2. In the TPD run hydrogen desorbed in a very complex way in four peaks at temperatures 327, 423, 555, and 715 K, respectively (curve 1), but its distribution was completely different when the catalyst was also exposed to CO (TPSR, curves 2–4). The second, large peak at 423 K was absent and a new, small peak at 490 K appeared. The third peak at 555 K was also missing and the fourth peak was significantly enlarged and shifted to 720–725 K, which was simultaneously the range of temperature for CO desorption (Fig. 1). The ratio of the amount of this strongly held H_2 to that of the strongly held CO (the peaks at about 720 K, Figs. 1 and 2) was within 0.52 to 0.58, indicating the

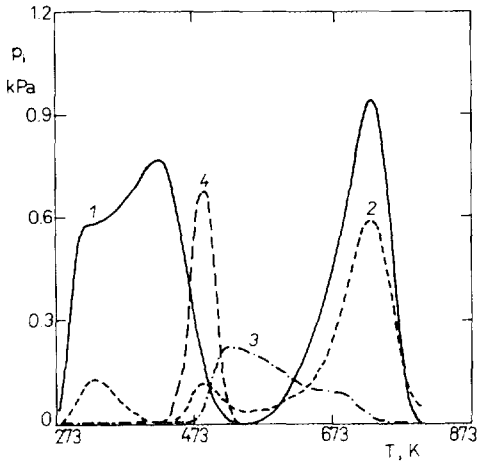

FIG. 3. Temperature-programmed reaction of CO coadsorbed with H_2. Curves: (1) CO; (2) H_2; (3) CH_4 (× 10); (4) H_2O (× 10). For conditions, see the Experimental section.

presence of a surface intermediate with approximate stoichiometry COH.

In parallel to carbon monoxide and hydrogen thermal desorption, methane and water were formed during TPSR, i.e., when CO and H_2 from 3% CO/H_2 mixture had been adsorbed on the catalyst surface. The products were typically evolved in a TPSR run as shown in Fig. 3. Simultaneous CO and H_2 desorption is also depicted. Water evolved always in one narrow peak at 490 K and methane in two broad peaks at approximately 525 and 685 K. The most significant observation was that water desorbed at lower temperature than methane and that the COH intermediate (see above) decomposed rather than giving methane and water. Therefore, CO and COH dissociated more easily than they were hydrogenated to CH_4.

Concentration Programmed Reaction

Two different types of stop and start-up transient experiments were performed. Either the CO/Ar mixture (CO disproportionation reaction) was replaced in a step manner by H_2, and vice versa, or the feed of CO/H_2 mixture (CO methanation reaction) was stepped to pure H_2.

$Ar \rightarrow CO/Ar \rightarrow H_2$ step change. Figure 4 shows the run where the activated catalyst was pretreated by hydrogen at 473 K, then by Ar, and finally the feed of Ar was switched to 13% CO/Ar mixture. After 1 min, this mixture was replaced by pure H_2. Following the step change from Ar to CO/Ar, CO was adsorbed, since a short induction period was observed before CO appeared in the gaseous phase. Simultaneously, a small amount of hydrogen desorbed from the catalyst surface, evidencing the replacement of H_2 with CO on the catalyst surface. Although some hydrogen had apparently been present on the catalyst surface, no methane was produced. The pressure of CO then quickly attained the steady-state value. When the feed was changed to pure hydrogen, a sharp peak of methane was seen simultaneously with a broader peak of water. The initial rate of the methane formation was significantly higher than that of water i.e., the rates of the methane and water formation were controlled by different reaction steps. If the purge by argon was inserted between the switch from CO/Ar to H_2 to remove CO from the gaseous phase, the initial rate of methane production

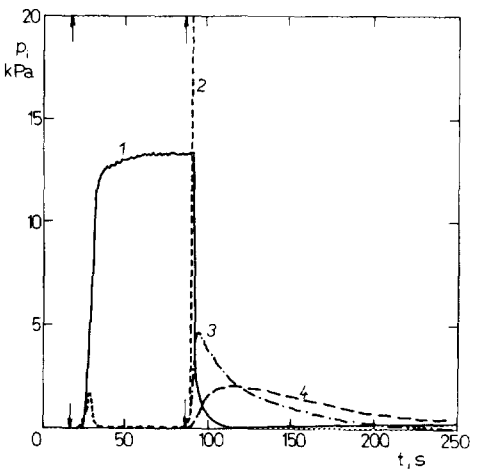

FIG. 4. Transient response to concentration step change Ar → 13% CO/Ar → H_2 at 473 K. Curves: (1) CO; (2) H_2; (3) CH_4; (4) H_2O. The switches are indicated by vertical arrows.

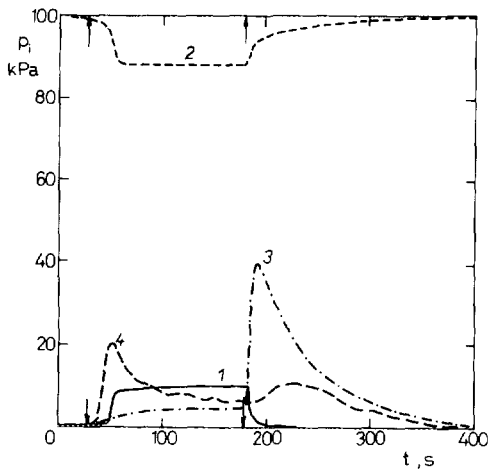

FIG. 5. Transient response to concentration step change ($H_2 \rightarrow$ 11% $CO/H_2 \rightarrow H_2$ at 458 K. Curves: (1) CO; (2) H_2; (3) CH_4 (× 10); (4) H_2O (× 10). The switches are indicated by vertical arrows.

was higher and less methane and water were produced. This result indicates competition of gaseous CO with H_2 for active surface after the direct CO/H_2 switch. The amount of CH_4 formed (as found from the area below the methane response curves) was about 25 μmol/g, well below the monolayer coverage (109 μmol/g). The same runs were performed at 518 and 533 K, and the transients and coverages were similar to those observed at 473 K.

$H_2 \rightarrow CO/H_2 \rightarrow H_2$ step change. In the range of 458–483 K, the transient responses were similar to each other and for 458 K are documented by Fig. 5. The responses were reproducible and no catalyst deactivation was observed. After a switch from H_2 to mixture containing 11% CO in H_2, hydrogen pressure quickly fell, and after a short induction period, carbon monoxide pressure increased. The pressure of methane increased gradually and levelled off at a steady-state value. The production of water passed through a sharp maximum followed by a slow decrease to steady state. The excess of water evolved (with respect to methane), establishes that after finishing the start-up period, the catalyst surface withholds some species not containing oxygen. The higher initial rate of water production in comparison with methane clearly shows that at this temperature, carbon monoxide splits and is hydrogenated to water much faster than is the rate of its hydrogenation to methane. When the feed was switched back to pure H_2, methane and water were immediately produced, with a higher rate of methane formation. The response was similar to that observed after the $CO/Ar \rightarrow H_2$ step change (Fig. 4).

When the reaction temperature was increased from 458 to 498 K, then after the step change from H_2 to 5% CO/H_2 mixture, methane and water were produced at comparable rates (Fig. 6), with a mild maximum on the water curve. The production of methane started several seconds before any water appeared. It follows that the rates of methane and water formation were probably controlled by the same process, i.e., the C–O bond splitting. The maximum on the water concentration may indicate that water is formed by more than one reaction. Following the backward switch to H_2, unlike the responses between 458 and 483 K, a monotonic decrease in the water production rate was observed, while the methanation

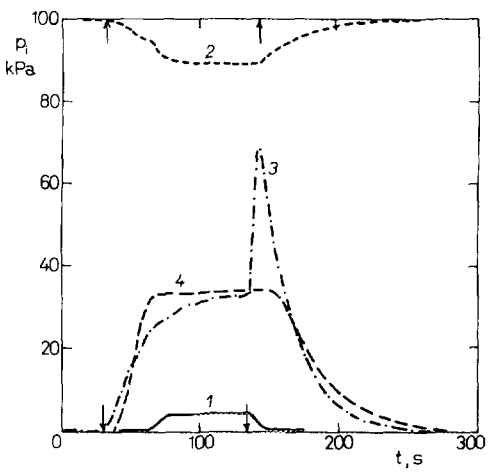

FIG. 6. Transient response to concentration step change $H_2 \rightarrow$ 5% $CO/H_2 \rightarrow H_2$ at 498 K. For curves, see Fig. 5. The switches are indicated by vertical arrows.

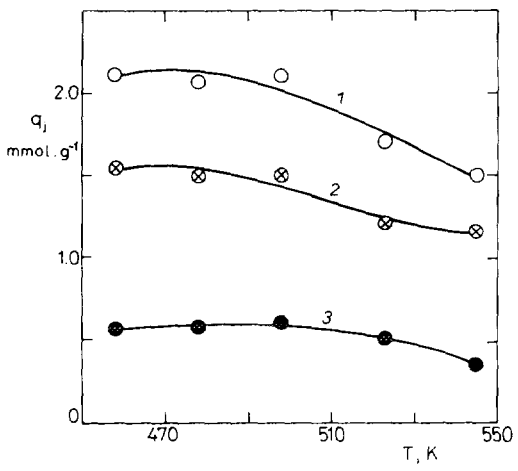

FIG. 7. Temperature dependence of evolved amounts of methane (1), water (3), and their difference (2) after switch to H_2. Methanation of 10% CO/H_2 mixture at the same temperature followed by 1-min purge by Ar preceded the switch.

rate passed through a pronounced maximum (Fig. 6).

The effect of purging the reactor by argon before the switch from the methanation reaction mixture back to hydrogen was investigated to estimate the effect of gaseous CO preserved in the reactor void volume on the methanation rate. The methane production rate was markedly higher, and less methane and water were produced due to the absence of CO in the gas phase. The observed increase of the initial methanation rate after removal of CO from the gas phase therefore stemmed from the poor ability of hydrogen to compete with CO for the surface sites.

By integration of the response curves for methane and water, the amounts of methane and water formed by hydrogenation of surface reaction intermediates were estimated to be between 458 and 545 K. In this way the amount of non-oxygenated methane and oxygenated water precursors on the catalyst surface could be determined. The result is shown in Fig. 7. The total amount of accumulated carbonaceous intermediates was much higher than after treatment of the catalyst by CO/Ar mixtures (about 25 μmol/g only, see above) and the prevailing surface species did not contain oxygen. The surface concentrations exceeded severalfold the monolayer capacity as estimated from H_2 adsorption. Hydrogen in the reaction mixture therefore made the deposition of reaction intermediates much easier. The deposition was fast and quickly finished as the amount of methane evolved remained practically the same when the time of exposure of the catalyst to methanation reaction mixture was increased from several seconds to minutes. No systematic experiments were performed on the influence of the reactant partial pressures on the deposition but, apparently, the amount of deposits was sensitive to the gas-phase composition.

The methods used in this work bring new important evidence about the methanation reaction behavior under unsteady-state reaction conditions. It is evident that description of the unsteady-state reaction behavior requires the following phenomena to be considered.

1. Carbon monoxide and hydrogen adsorb competitively on at least two types of catalyst surface sites. Carbon monoxide can replace adsorbed hydrogen by a substitution mechanism.

2. Hydrogen enables fast and massive multilayer deposition of oxygenated and nonoxygenated carbonaceous reaction intermediates to occur.

3. Most of these intermediates are formed and react under unsteady-state reaction conditions but are unreactive at the steady state. Their amounts depend on the reaction conditions.

4. Carbon monoxide inhibits hydrogenation of deposits through blocking the surface to hydrogen. Hydrogen apparently needs some free sites to form an adsorbed form, i.e., it is not able to remove (hydrogenate) adsorbed CO by a substitution mechanism.

These effects are not considered in the steady-state methanation reaction schemes and kinetics given in the literature, which are usually based on the simple Langmuir–Hinshelwood models. Recently, we

described[32] the steady-state methanation on the G-33 catalyst by the following reaction scheme (s_1 is an active site):

$$\begin{aligned} H_2 + 2s_1 &= 2H \cdot s_1 \\ CO + s_1 &= CO \cdot s_1 \\ CO \cdot s_1 + 2H \cdot s_1 &\rightarrow CH_2 \cdot s_1 + O \cdot s_1 + s_1 \\ CH_2 \cdot s_1 + 2H \cdot s_1 &= CH_4 + 3s_1 \\ O \cdot s_1 + 2H \cdot s_1 &= H_2O + 3s_1. \end{aligned} \quad (A)$$

Under unsteady state, the existence of another type of surface site, s_2, should be considered as evidenced by the above adsorption and TPR measurements. At steady state these sites are blocked by carbonaceous intermediates which do not react, owing to poor access of hydrogen to the catalyst surface. It is, therefore, speculated that the following reactions (B) could proceed on sites s_2 to give the unsteady-state surface intermediates:

$$\begin{aligned} H_2 + 2s_2 &= 2H \cdot s_2 \\ CO + 2s_2 &= C \cdot s_2 + O \cdot s_2 \\ CO + H \cdot s_2 &= COH \cdot s_2 \\ CO + 2H \cdot s_2 &= C \cdot s_2 + O \cdot s_2 + H_2 \\ CO + 2H \cdot s_2 &= CO \cdot s_2 + s_2 + H_2 \\ O \cdot s_2 + 2H \cdot s_2 &= H_2O + 3s_2 \\ C \cdot s_2 + 2H \cdot s_2 &= CH_2 \cdot s_2 + 2s_2 \\ CH_2 \cdot s_2 + 2H \cdot s_2 &= CH_4 + 3s_2. \end{aligned} \quad (B)$$

The first reaction activates hydrogen for unsteady-state reactions. It is also probable that CO adsorbs/disproportionates on sites s_2 (second step). CO substitutes hydrogen by the following three reactions, the products of which gradually block the sites s_2 for the access of hydrogen. The last three reactions produce methane and water at unsteady-state, as indicated in Fig. 6. The unsteady-state multilayer deposition of reaction intermediates can be formalized with the help of reactions (C):

$$\begin{aligned} COH \cdot s_2 + H \cdot s_2 &= C_s + H_2O + 2s_2 \\ CO + 2H \cdot s_2 &= C_s + H_2O + 2s_2 \\ CO \cdot s_2 + 2H \cdot s_2 &= C_s + H_2O + 3s_2 \\ C_s + CO &= CO \cdot C_s. \end{aligned} \quad (C)$$

The first two reactions produce multilayer carbon C_s on which CO can absorb similarly as in CO adsorption on active carbon. At this range of reaction temperatures, carbon can be deposited in a multilayer form as polymeric or amorphous carbon able to dissolve in and penetrate through nickel (*33*, *34*). Massive multilayer deposition of carbonaceous species is apparent from the comparison of the adsorption (monolayer) capacity of 109 μmol g^{-1} (see Table 2) and the evolved amount of methane of about 2000 μmol g^{-1} during TPSR (Fig. 7). Oxygen-containing deposits may involve CO adsorbed on the carbon surface indicated by IR spectroscopy (*35*). These intermediates can also be deposited on the surface of the SiO_2 support, which remains uncovered by nickel even at high nickel loading. C and CO can be transported on the catalyst support by surface (spillover) or bulk migration (*34*, *36*). When the feed is switched to hydrogen then hydrogen can be activated on sites s_2 via the back-substitution reaction and multilayer unsteady-state deposits are hydrogenated to methane and water, e.g., by reactions (D):

$$\begin{aligned} C_s + 2H \cdot s_2 &= CH_2 \cdot s_2 + s_2 \\ CH_2 \cdot s_2 + 2H \cdot s_2 &= CH_4 + 3s_2 \\ CO \cdot C_s + 2H \cdot s_2 &= CO \cdot s_2 \\ &\quad + CH_2 \cdot s_2, \ldots, \text{etc.} \end{aligned} \quad (D)$$

We believe that the schemes presented allow us to explain the enhancement of the reaction rate above the values attainable under steady-state conditions by a variation of the reactant concentrations in the feed, which we observed in our parallel work (*37*). It appears that the basic prerequisite of the enhancement is the storage of reaction intermediates on sites other than steady-state reaction ones in amounts dependent on the reaction conditions. Those deposits can be formed only under the presence of CO. On the other hand, carbonaceous deposits can be removed (hydrogenated) only if CO is missing (or present in a very small concentration) in the gas phase. These contradic-

tory requirements can be fulfilled only under dynamic conditions (switching CO rich ⇆ CO lean mixtures). CO is able to remove H_2 from the surface via the substitution mechanism (steps B-4, 5) without any free sites s_2. For similar action (CO removal) hydrogen needs some free sites s_2 where it forms $H \cdot s_2$ and then "cleans" the surface (step C-3) increasing in such a way the catalyst activity. The catalyst activity becomes effectively variable and cannot be taken as a constant. Simultaneously, the existence of different adsorption/reaction sites for hydrogen and carbon monoxide with the substitution mechanism for CO adsorption must be considered, as otherwise the above storage would be small due to adsorption of hydrogen. In this way the catalytically active surface saturated by one reaction component still remains accessible to another reaction component and the unsteady-state deposits can survive on the surface at steady state.

REFERENCES

1. Mori, T., Masuda, H., and Imai, H., *J. Phys. Chem.* **86,** 2753 (1982).
2. Underwood, R. P., and Bennett, C. O., *J. Catal.* **86,** 245 (1984).
3. Lee, P.-I., and Schwarz, J. A., *Ind. Eng. Chem. Process. Des. Dev.* **25,** 76 (1986).
4. Van Ho, S., and Harriott, P., *J. Catal.* **64,** 272 (1980).
5. Cant, N. W., and Bell, A. T., *J. Catal.* **73,** 257 (1982).
6. Krebs, H. J., Bonzel, H. P., and Gafner, G., *Surf. Sci* **88,** 269 (1979).
7. Biloen, P., and Sachtler, W. M. H., in "Advances in Catalysis (D. D. Eley, H. Pines, and P. B. Weisz, Eds.), Vol. 30, p. 165. Academic Press, New York, 1981.
8. Araki, M., and Ponec, V., *J. Catal.* **44,** 439 (1976).
9. Goodman, D. W., Kelley, R. D., Madey, T. E., and White, J. M., *J. Catal.* **64,** 479 (1980).
10. Biloen, P., *J. Mol. Catal.* **21,** 17 (1983).
11. Coenen, J. W. E., van Nisselrooy, P. F. M. T., de Croon, M. H. M. J., van Dooren, P. F. H. A., and van Meerten, R. Z. C., *Appl. Catal.* **25,** 1 (1986).
12. Ponec, V., *Catal. Rev.* **18,** 151 (1978).
13. van Barneveld, W. A. A., and Ponec, V., *J. Catal.* **51,** 426 (1978).
14. Ekerdt, J. G., and Bell, A. T., *J. Catal.* **58,** 170 (1979).
15. Frost, A. C., Elek, L. F., Chang-Lee, Y., and Rabo, J. A., *Energy Prog.* **2,** 247 (1982).
16. Frost, A. C., Elek, L. F., Chang-Lee, Y., Risch, A. P., and Rabo, J. A., *Appl. Catal.* **2,** 347 (1982).
17. Dalla Betta, R. A., and Shelef, M., *J. Catal.* **49,** 383 (1977).
18. Kellner, C. S., and Bell, A. T., *J. Catal.* **67,** 175 (1983).
19. van Nisselrooy, P. F. M. T., Luttikholt, J. A. M., van Meerten, R. Z. C., de Croon, M. H. M. J., and Coenen, J. W. E., *Appl. Catal.* **6,** 271 (1983).
20. Biloen, P., Helle, J. N., van den Berg, F. G. A., and Sachtler, W. M. H., *J. Catal.* **58,** 95 (1979).
21. Biloen, P., Helle, J. N., van den Berg, F. G. A., and Sachtler, W. M. H., *J. Catal.* **81,** 450 (1983).
22. Happel, J., Suzuki, I., Kokayeff, P., and Fthenakis, V., *J. Catal.* **65,** 59 (1980).
23. Happel, J., Cheh, H. Y., Otarod, M., Ozawa, S., Severdia, A. J., Yoshida, T., and Fthenakis, V., *J. Catal.* **75,** 314 (1982).
24. Galuzska, J., Chang, J. R., and Amenomiya, Y., *in* "Proceedings, 7th Intern. Congress on Catalysis, Tokyo, 1980" (T. Seiyama and K. Tanabe, Eds.), Part A, p. 529, Kodansha/Elsevier, Tokyo/Amsterdam, 1981.
25. Zagli, E., Falconer, J. L., and Keenan, C. A., *J. Catal.* **56,** 453 (1979).
26. Ozdogan, S. Z., Gochis, P. D., and Falconer, J. L., *J. Catal.* **83,** 257 (1983).
27. Kester, K. B., and Falconer, J. L., *J. Catal.* **89,** 380 (1984).
28. Kester, K. B., Zagli, E., and Falconer, J. L., *Appl. Catal.* **22,** 311 (1986).
29. McCarty, J. G., and Wise, H., *J. Catal.* **57,** 406 (1979).
30. Hayes, R. E., and Ward, K. J., *Appl. Catal.* **20,** 123 (1986).
31. Stuchlý, V., and Klusáček, K., *Collect. Czech. Chem. Commun.* **55,** 354 (1990).
32. Stuchlý, V., and Klusáček, K., *Collect. Czech. Chem. Commun.*, in press.
33. Trimm, D. L., *Catal. Rev.—Sci. Eng.* **16,** 155 (1977).
34. Bartholomew, C. H., *Catal. Rev.—Sci. Eng.* **24,** 67 (1982).
35. Low, G. G., and Bell, A. T., *J. Catal.* **57,** 397 (1979).
36. Kapoor, A., Yang, R. T., and Wong, C., *Catal. Rev.—Sci. Eng.* **31,** 129 (1989).
37. Stuchlý, V., and Klusáček, K., *in* Proceedings, International Conference on Unsteady-State Processes in Catalysis, Novosibirsk, 1990," p. 423, VSP Publishers, Utrecht, The Netherlands.